


<b>Titre:</b> Title:	Determination of critical state line (CSL) for silty-sandy iron ore tailings subjected to low-high confining pressures
<b>Auteurs:</b> Authors:	Nilo César Consoli, João Vítor de Azambuja Carvalho, Alexia Cindy Wagner, Hugo Carlos Scheuermann Filho, Inácio Carvalho, Pedro Cacciari, & João Paulo de Sousa Silva
<b>Date:</b>	2023
<b>Type:</b>	Article de revue / Article
<b>Référence:</b> Citation:	Consoli, N. C., Carvalho, J. V. A., Wagner, A. C., Filho, H. C. S., Carvalho, I., Cacciari, P., & Silva, J. P. S. (2023). Determination of critical state line (CSL) for silty-sandy iron ore tailings subjected to low-high confining pressures. Journal of Rock Mechanics and Geotechnical Engineering, 13 pages. <a href="https://doi.org/10.1016/j.jrmge.2023.06.014">https://doi.org/10.1016/j.jrmge.2023.06.014</a>

 **Document en libre accès dans PolyPublie**  
Open Access document in PolyPublie

<b>URL de PolyPublie:</b> PolyPublie URL:	<a href="https://publications.polymtl.ca/56692/">https://publications.polymtl.ca/56692/</a>
<b>Version:</b>	Version officielle de l'éditeur / Published version Révisé par les pairs / Refereed
<b>Conditions d'utilisation:</b> Terms of Use:	CC BY-NC-ND

 **Document publié chez l'éditeur officiel**  
Document issued by the official publisher

<b>Titre de la revue:</b> Journal Title:	Journal of Rock Mechanics and Geotechnical Engineering
<b>Maison d'édition:</b> Publisher:	Elsevier BV
<b>URL officiel:</b> Official URL:	<a href="https://doi.org/10.1016/j.jrmge.2023.06.014">https://doi.org/10.1016/j.jrmge.2023.06.014</a>
<b>Mention légale:</b> Legal notice:	



Contents lists available at ScienceDirect

# Journal of Rock Mechanics and Geotechnical Engineering

journal homepage: [www.jrmge.cn](http://www.jrmge.cn)

## Full Length Article

# Determination of critical state line (CSL) for silty-sandy iron ore tailings subjected to low-high confining pressures

Nilo Cesar Consoli<sup>a,\*</sup>, João Vítor de Azambuja Carvalho<sup>a</sup>, Alexia Cindy Wagner<sup>a</sup>, Hugo Carlos Scheuermann Filho<sup>a</sup>, Inácio Carvalho<sup>b</sup>, Pedro Pazzoto Cacciari<sup>b,c</sup>, João Paulo de Sousa Silva<sup>b</sup>

<sup>a</sup> Civil Engineering, Universidade Federal do Rio Grande do Sul, Porto Alegre, RS, 90035-190, Brazil

<sup>b</sup> Exploration and Mineral Projects—Mineral Development Centre, VALE S.A., Santa Luzia, MG, 33040-900, Brazil

<sup>c</sup> Department of Civil, Geological and Mining Engineering, Polytechnique Montreal, Quebec, H3C 3A7, Canada

## ARTICLE INFO

### Article history:

Received 9 March 2023

Received in revised form

18 April 2023

Accepted 15 June 2023

Available online xxx

### Keywords:

Tailings

Iron ore tailings

dry stacking

Silty-sandy material

Critical state soil mechanics

High confining pressures

Particle breakage

## ABSTRACT

The disposal of filtered tailings in high dry stacks can induce particle breakage, changing the material's behaviour during the structure's lifetime. The grading changes influence material properties at the critical state, and this is not mature for intermediate artificial soils (tailings) in a broad range of confining pressures. In this paper, it aims to describe the behaviour of iron ore tailings in a spectrum of confining pressures broader than the reported in previous studies. A series of consolidated drained (CD) triaxial tests was carried out with confining pressures ranging from 0.075 MPa to 120 MPa. These results show that the amount of breakage plays an essential role in the response of iron ore tailings. The existence of curved critical state line (CSL) in both specific volume ( $v$ )–logarithm of mean effective stress ( $p'$ ) and deviatoric stress ( $q$ )–mean effective stress ( $p'$ ) planes, and different responses in the deviatoric stress–axial strain–volumetric strain curves were verified. An inverse S-shaped equation was proposed to represent the silty-sandy tailings' behaviour up to high pressures on  $v$ – $\ln p'$  plane. The proposed equation provides a basis for enhancing constitutive models and considers the evolution of the grading up to severe loading conditions. The adjustment considered three regions with different responses associated with particle breakage at different pressure levels.

© 2023 Institute of Rock and Soil Mechanics, Chinese Academy of Sciences. Production and hosting by Elsevier B.V. This is an open access article under the CC BY-NC-ND license (<http://creativecommons.org/licenses/by-nc-nd/4.0/>).

## 1. Introduction

Most engineering applications of geomaterials are limited to confining pressures around 1 MPa. The behaviour of these materials has been extensively studied up to this confinement level. However, some cases involve much higher pressures, e.g. at the tips of deep-driven piles, buried holes for petroleum extraction, high earth dams, or even in soils subjected to explosions or projectiles impacts (Leung et al., 1996; Xiao et al., 2016; Mun and McCartney, 2017; Yu, 2021). In the mining industry, high-pressure problems may arise for high dry stack facilities when exploring new disposal methods for the waste derived from extraction and processing (termed tailings).

Concerning dry stacking, the tailings are filtered to achieve the optimum moisture content and compacted in field to a defined compaction degree (Wu, 2020; Consoli et al., 2022). The stacks usually have distinct compaction states in different regions to follow the production rate of mining tailings (Davies, 2011; Lupo and Hall, 2011). Such structures may achieve heights of more than 300 m, which requires an understanding of the tailings' behaviour when subjected to high pressures, which are much higher than those achieved in typical geotechnical engineering applications.

The iron ore tailings can exhibit non-plastic behaviour, although they contain fines (basically silt size particles). It is well known that particulate materials present volumetric strains when subjected to shearing, up to a point in which shear strains occur without further volumetric or mean effective pressure changes (e.g. Consoli 1991; Been et al. 1991). This condition, known as the critical state, is stress-dependent and originates a locus of critical states depending on the stress level. Several works highlight the need for describing

\* Corresponding author.

E-mail address: [consoli@ufrgs.br](mailto:consoli@ufrgs.br) (N.C. Consoli).

Peer review under responsibility of Institute of Rock and Soil Mechanics, Chinese Academy of Sciences.

<https://doi.org/10.1016/j.jrmge.2023.06.014>

1674-7755 © 2023 Institute of Rock and Soil Mechanics, Chinese Academy of Sciences. Production and hosting by Elsevier B.V. This is an open access article under the CC BY-NC-ND license (<http://creativecommons.org/licenses/by-nc-nd/4.0/>).

such material's behaviour based on its states (e.g. Wroth and Bassett 1965; Been and Jefferies 1985; Poorooshasb 1989; Consoli 1991).

The theoretical framework captures the effects of both initial density and mean effective stress, and describes different states in which the material can exist, which is termed as the critical state soil mechanics (CSSM) (Schofield and Wroth, 1968). Its principles are usually employed in the constitutive modelling of geomaterials and have been extensively used in the development of mathematical models in both clayey and granular materials (e.g. Roscoe et al., 1958; Wroth and Bassett, 1965; Schofield and Wroth, 1968; Poorooshasb, 1989; Consoli, 1991; Yu, 1998; Gajo and Muir Wood, 1999a, b; Dafalias and Manzari, 2004).

Nonetheless, particle breakage can occur in granular materials subjected to sufficient high pressures, playing a major role in their mechanical responses (e.g. Coop 1990; Russell and Khalili 2004; Consoli et al., 2007; Mun and McCartney 2017). This evolution of the material's grading impacts the states achieved in a stress-density space as the packing of the particles can be more efficient when breakage occurs, changing the critical state location in the specific volume ( $\nu$ )–logarithm of mean effective stress ( $p'$ ) plane (Muir Wood and Maeda, 2008). Hence, the effects of changing the critical state location in the  $\nu$ – $\ln p'$  plane must be considered in the constitutive description of geomaterials.

Concerning the modelling of geomaterials with evolving grading, Muir Wood and Maeda (2008) defined three essential aspects: a quantitative measurement of the current grading state, an evolution law describing how this index changes, and rules which define the effect of changing grading on the material's mechanical responses. The authors also proposed a grading index ( $I_g$ ) and a definition of critical states in a space composed of the grading index, void ratio, and mean effective stress. The theory of Muir Wood (2017) accounted for different grading evolution possibilities, e.g. particle breakage and seepage transportation. However, when particle breakage is the only grading evolution phenomenon, the critical state line (CSL) becomes a trace of the proposed surface and could be represented in  $\nu$ – $\ln p'$  plane.

Several authors have presented idealised mathematical expressions to describe the locus of critical states in the compression plane, varying from simple semi-log linearisation to bi-linear (Been et al., 1991; Verdugo, 1992) or even tri-linear (Russell and Khalili, 2004) and high-order functions as power laws (Gudehus, 1996; Jefferies and Been, 2016). In their majority, the existent constitutive models could be used in conjunction with any idealised expressions. Jefferies and Been (2016) suggested that the choice of the idealised equation, from a mathematical standpoint, is simply a matter of which best fits the data. However, the equations proposed in the literature do not fit well with the broader pressure spectrum data, which involve non-continuous definitions or depend upon too many parameters. The CSL tends to change with particle crushing. Then, the constitutive models that include the CSL as a fundamental feature controlling strength and dilatancy will be affected by the possibility of a dynamically changing CSL. Thus, it is important to incorporate the grading evolution in the models considering the behaviour over a wide range of pressures (Muir Wood and Maeda, 2008).

Accordingly, this paper aims to describe behaviour of iron ore tailings on a broader spectrum of pressures than those reported in the literature. For this, consolidated drained (CD) triaxial tests are conducted with confining pressures up to 120 MPa. The specimens' stress-strain response is evaluated for the full range of pressures tested, and the results are analysed in the light of CSSM. Finally, a new equation accounting for the experimentally observed behaviour is proposed.

## 2. Experimental program

The experimental program was carried out in three parts. First, the physical characteristics of the iron ore tailings were determined, and 14 drained triaxial compression tests were conducted over a wide range of pressures. Then, the possibility of particle breakage during the shearing was assessed by means of particle size distribution (PSD) and scanning electron microscope (SEM) images, both conducted on representative untested and after sheared specimens. Finally, the results were analysed in the light of the CSSM, and a new equation was proposed to represent the CSL on the  $\nu$ – $\ln p'$  plane. As a complement, one isotropic compression test up to 120 MPa also was carried out to evaluate particle breakage.

### 2.1. Materials

The studied iron ore tailings were obtained from a mine in the Quadrilátero Ferrífero (iron quadrangle) region located at the province of Minas Gerais, southeast of Brazil. The PSD was obtained via sieve and sedimentation analysis in accordance with ASTM D7928 (2021). Fig. 1 shows the PSD (0.3% of medium sand, 51.8% of fine sand, 46.5% of silt, and 1.5% of clay size), from which it can be seen that the untested tailings specimen is well-graded (coefficient of curvature ( $C_{cu}$ ) of 1.98 and coefficient of uniformity ( $C_u$ ) of 10). The Atterberg limits (non-plastic tailings) and the specific gravity ( $G_s = 3.05$ ) were evaluated, respectively, in accordance with ASTM D4318-17 (2017) and ASTM D854-14 (2014). The compaction characteristics were assessed using both the standard (optimum moisture content ( $w_{opt}$ ) = 11.5% and maximum dry unit weight ( $\gamma_{dmax}$ ) = 19.3 kN/m<sup>3</sup>) and modified efforts ( $w_{opt}$  = 10.0% and  $\gamma_{dmax}$  = 20.2 kN/m<sup>3</sup>) according to ASTM D698 (2021) and ASTM D1557 (2021), respectively. The minimum ( $e_{min}$  = 0.36) and maximum void ratios ( $e_{max}$  = 1.28) were evaluated based on ASTM D4254-16 (2016) and ASTM D4253-16 (2016), respectively.

In accordance with the Unified Soil Classification System (ASTM D2487-17, 2017) the material is classified as silty sand (SM). Mineralogically, the iron ore tailings are mainly composed of quartz (76.2%), iron oxide (20.9%), feldspar (1.4%), amongst other minerals in tiny amounts. The mineralogy was carried out by an associated analysis of X-ray diffraction (XRD) test and SEM with two energy-dispersive spectroscopy (SEM-EDS), which has enabled the quantification of the mineral phases.

Unlike natural soils, where the grading and the fabric mainly arise from transportation and sedimentation over elapsed time, these characteristics of tailings are mainly affected by the beneficiation process. Hence, the iron ore tailings are composed of a broad range of grain sizes producing a fabric where the smaller particles involve the greater ones. As well, these tailings present unique particles shapes (e.g. flatten and with marked angularities) as can be seen in the SEM micrographs displayed in Fig. 2a.

### 2.2. Testing methods

The testing program has required using two triaxial apparatuses due to the high pressures applied. The tests under usual confining pressures were carried out in a conventional triaxial apparatus (considering saturated specimens), and those subjected to higher confining pressures were conducted on dry specimens using a high-pressure triaxial apparatus, as listed in Table 1. In both cases, cylindrical specimens (50 mm in diameter and 100 mm in height) were adopted. For tests on saturated specimens, the specimens were moulded through moist tamping (e.g. Suits et al., 2003; Corrêa and Oliveira Filho 2019). For this, wet tailings layers were deposited

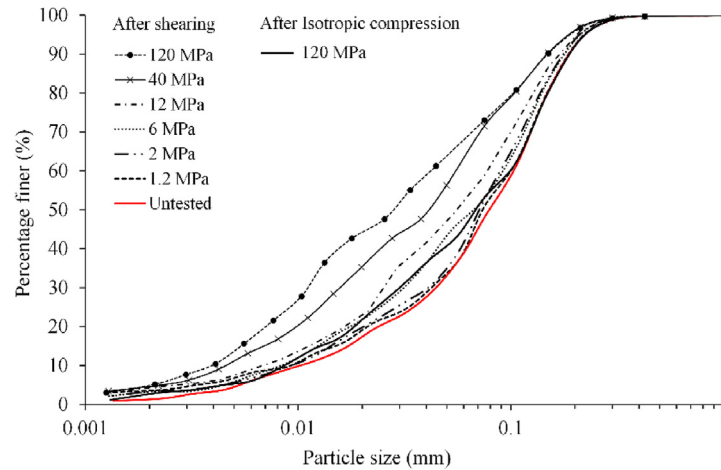


Fig. 1. PSD of the untested and tested iron ore tailings.

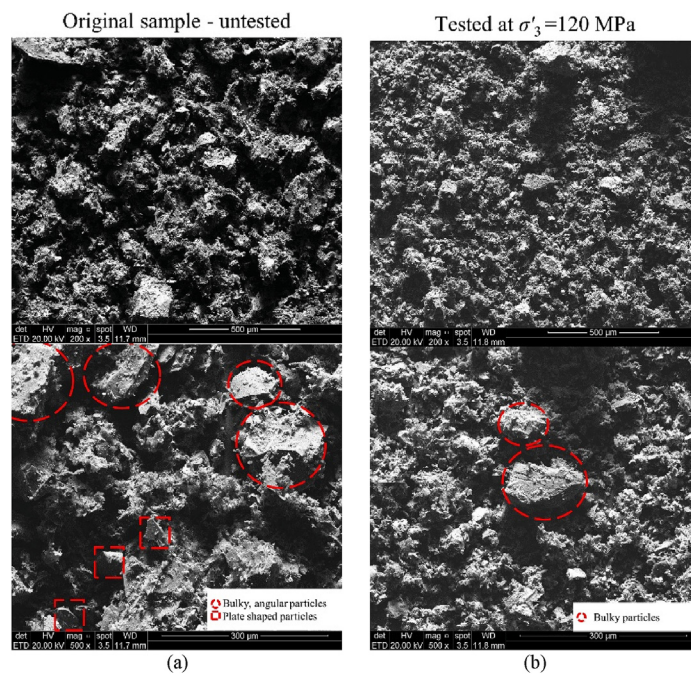


Fig. 2. SEM images of tailings (a) before and (b) after testing at 120 MPa confining pressure.

inside a split mould and tamped manually to the assigned degree of compaction (dense or loose according to defined in Table 1) and a moisture content ( $w$ ) of 11.5%. Five layers were used in this process, and the top of the first four layers was scarified to guarantee the adherence of the subsequent layer. The saturation stage comprehended  $\text{CO}_2$  percolation, followed by water percolation and finally application of back-pressure increments until a Skempton  $B$ -value is greater than 0.98, indicating specimen full saturation. The consolidation phase was conducted by incrementing the chamber pressure at a rate of 0.05 MPa/h up to the desired  $\sigma'_3$  (minor confining effective stress) value. This rate was adequate, as no excess pore pressure was generated during this procedure. Once the consolidation was terminated, the strain-controlled shearing started at a rate of 1.5 mm/h.

On the other hand, specimens containing no moisture were used for the higher confining pressures. These samples were dried in an oven for 24 h at 105 °C to guarantee the zero-moisture content

condition. For dry moulding, a pre-established mass of dry tailings was deposited inside a split mould and manually tapped (even slightly vibrated) to the assigned dry density (100% of the standard effort). In this case, only dense samples were used due to the high-pressure and the need to use internal measurements for calculations of volumetric change. Fig. 3 presents a schematic diagram of the high-pressure triaxial system used. The isotropic compression phase of the high-pressure triaxial compression tests consisted of incrementing the chamber pressure at a constant rate up to the desired  $\sigma'_3$  value. Then, the shearing started using a strain-controlled setup at a rate of 1.5 mm/h.

Internal measurements allowed the assessment of the volumetric strains during the entire isotropic compression phase and the beginning of the shearing for tests on dry specimens. The axial and circumferential strains were measured by the MTS in-vessel extensometer kit. This kit is designed for measuring axial and circumferential strains on a cylindrical specimen, loaded in a high-

**Table 1**  
Results of drained triaxial tests.

ID (Confining pressure)	Initial state	Test Condition	After compression		End of the test					
			Confining pressure, $p'_0$ (kPa)	Specific Volume, $\nu$	Mean effective stress, $p'$ (kPa)	Deviatoric stress, $q$ (kPa)	Specific volume, $\nu$	Stress ratio ( $\eta = q/p'$ )	Friction angle, $\phi'$ ( $^\circ$ ) <sup>a</sup>	Relative breakage
0.20 MPa	Loose	Saturated	200	1.75	378.78	538.32	1.65	1.42	35.07	-
0.40 MPa	Loose	Saturated	400	1.73	757.91	1075.99	1.62	1.42	35.03	-
0.80 MPa	Loose	Saturated	800	1.7	1507.39	2119.7	1.59	1.41	34.72	-
1.60 MPa	Loose	Saturated	1600	1.65	3000.04	4196.65	1.54	1.4	34.55	-
0.075 MPa	Dense	Saturated	75	1.54	162.2	260.34	1.59	1.61	39.28	-
0.10 MPa	Dense	Saturated	100	1.54	200.74	302.21	1.61	1.51	37	-
0.15 MPa	Dense	Saturated	150	1.53	308.19	472.01	1.58	1.53	37.59	-
0.90 MPa	Dense	Saturated	900	1.52	1774.76	2618.27	1.55	1.48	36.3	-
1.20 MPa	Dense	Dry	1200	1.52	2323.98	3369.09	1.57	1.45	35.72	0.04
2 MPa	Dense	Dry	2000	1.51	3840.68	5524.24	1.54	1.44	35.46	0.07
6 MPa	Dense	Dry	6000	1.5	11765.7	17301.16	1.39	1.47	36.19	0.12
12 MPa	Dense	Dry	12000	1.46	23002.09	33005.29	1.36	1.43	35.38	0.2
40 MPa	Dense	Dry	40000	1.39	72887.39	98558.18	1.27	1.35	33.49	0.35
120 MPa	Dense	Dry	120000	1.31	215847.82	287547.03	1.21	1.33	33.03	0.4

<sup>a</sup> Friction angles for the individual tests were obtained by considering  $\phi' = \arcsin[(3\eta)/(6+\eta)]$ .

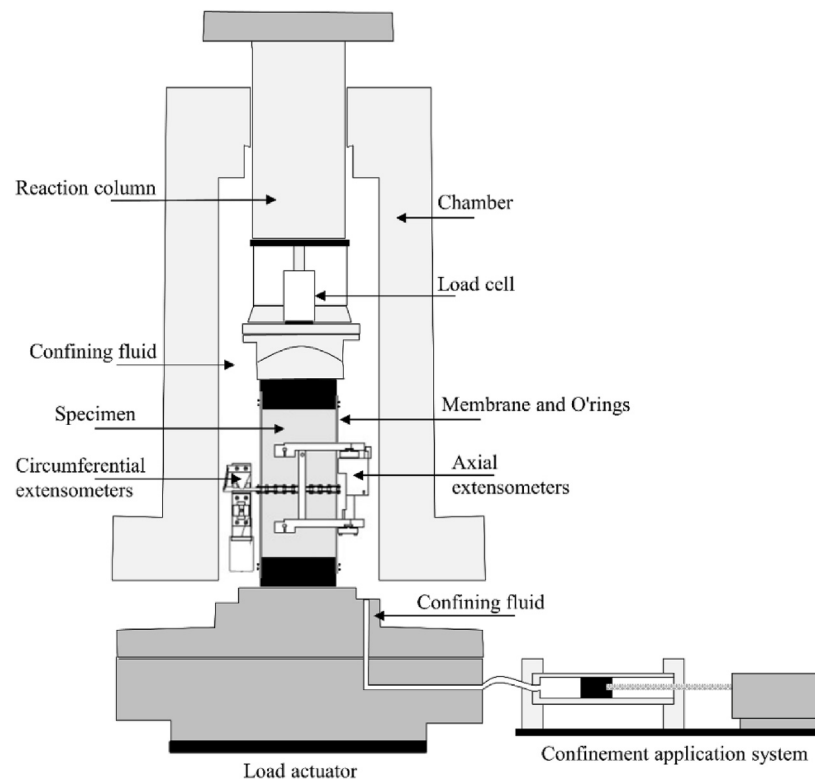


**Fig. 3.** Schematic diagram of the high-pressure triaxial system.

pressure vessel (up to 140 MPa). The axial strain was calculated by the average of two axial extensometers (+5/−2.5 mm maximum travel) fixed in opposed positions. The circumferential strain was calculated by a chain system, which measures the circumference change deformation during test (±3.75 mm maximum chordal travel). The chain was positioned in the middle of the specimen, between the extremities of axial extensometers. An in-vessel load cell (with spherical seat) provided the direct measurement of specimen deviatoric load (up to 2600 kN).

In shearing, after the valid interval for the internal extensometer measurements had finished, the volumetric strains were assessed by the variation in the triaxial cell chamber confining fluid

(Mun and McCartney, 2015, 2017; Ahmadi-Naghadeh and Toker, 2017). This was achieved by controlling the piston displacement inside the confinement application system (1  $\mu\text{m}$  transducer resolution). Thus, the volume change of the specimen was evaluated by a conjunction of internal and external measurements. Mun and McCartney (2017) performed triaxial isotropic compression tests on dry sands up to high pressures. The authors found similar behaviour in compression to that usually reported for saturated sands, indicating the accuracy of the test method. Furthermore, all analyses presented in this study refer to effective stresses and the consideration of completely dry or saturated specimens are not expected to differ.

### 3. Results and discussion

#### 3.1. Compression behaviour

The compression behaviour was assessed considering the isotropic compression phase of two triaxial tests. The loose and dense samples were isotropically compressed to the higher pressures (1.6 MPa and 120 MPa, respectively). Fig. 4 shows both compression paths starting from the two different initial conditions. Although the loose specimen was less stiff than the dense one, they both presented a converging trend to a unique normal compression line (NCL).

#### 3.2. Shearing behaviour

A series of drained triaxial compression tests was performed on iron ore tailings at various confining pressures between 0.075 MPa and 120 MPa to obtain the shape of the CSL. In addition, these tests were useful in evaluating the overall stress-strain response and volume change behaviour of iron ore tailings in triaxial compression. Table 1 summarises the details of the tests conducted.

Fig. 5a shows the triaxial compression normalised deviatoric stress ( $q/p'_0$ )–axial strain behaviour of tests carried out on loosely moulded specimens. Loose samples were selected to better define the CSL for low stresses since dense tests usually show strain localisation during the shearing at these stress levels, making it difficult to define the CSL. The volumetric strains that occurred during shearing were compressive for all these tests. The volumetric strain magnitude was similar for the specimens tested at 0.4 MPa, 0.8 MPa, and 1.6 MPa confining pressures. This result indicates that these samples were in a similar state parameter at the start of the shearing (Been and Jefferies 1985). Despite the tests having different void ratios and confining pressures after consolidation, they reached a similar maximum normalised deviatoric stress, and no peak stress was noted.

Fig. 5b shows the normalised deviatoric stress–axial strain and volumetric behaviour for the iron ore tailings at initial dense states. The normalised deviatoric stress ( $q/p'_0$ ) is presented to properly show the variation in the shapes of the deviatoric stress–axial strain curves over the wide range of utilised confining pressures.

Lower confining pressure tests (0.075 MPa, 0.1 MPa, and 0.15 MPa) show normalised deviatoric stress–axial strain curves that rise quickly to peak stress. These tests exhibit the largest

normalised deviatoric stress value and the smallest axial strain at the peak among all tests. Concerning the volumetric change, the volumetric strains are initially compressive and then predominantly dilatant.

With the increase in confining pressure (0.9 MPa, 1.2 MPa, and 2 MPa), the initial gradient of the normalised deviatoric stress–axial strain curves tends to decrease, and the peak occurs at a higher axial strain with lower normalised deviatoric stress. Also, the volumetric strains become initially more compressive because higher confining pressure constrains the sample dilation. The increase in confining pressure equal and above 6 MPa causes the initial slope of the stress-strain curves to flatten (steepness decreases), the maximum normalised deviatoric stress to decrease (there is no peak), an increase of the axial strain at the maximum stress, and more volumetric compression (there is no dilatant tendency). The flattening of the stress-strain curve is mainly observed in higher pressure tests. The stress-strain curves at higher stresses may be divided into three zones: an initial steep linear portion, a long middle linear portion, and an almost horizontal portion near the maximum stress.

Fig. 6 shows the stress paths of the iron ore tailings on the  $q$ – $p'$  plane with the final points at the critical state up to low (see Fig. 5a), high (see Fig. 5b), and extremely high (see Fig. 5c) mean effective stresses. Although there are only a few points for high and extremely high pressures, separating the pressure ranges allows the observation of critical state strength evolution under each condition. The increase in mean effective stress reflects an increase in the maximum deviatoric stress. However, the increase of  $q$  compared to  $p'$  is not proportional, and the material shows a remarkable nonlinear behaviour for high confining pressure values. The same trend is observed in Fig. 7 by plotting the stress ratio ( $\eta$ ) versus axial strain ( $\epsilon_a$ ) in which it might be observed that the final stress ratio depended upon the confinement level. The  $\eta$  ( $=q/p'$ ) values on the end of test obtained varied from 1.6 to 1.3, corresponding to a variation in the friction angle from  $39^\circ$  to  $33^\circ$ . The specific values for each test can be seen in Table 1. The friction angle in compression decreases with increasing confining pressures (up to 40 MPa) and tends to stabilise at higher confining pressures (120 MPa).

#### 3.3. Particle breakage analysis

PSD analyses were carried out with untested tailings sample and representative samples retrieved from specimens sheared at confining pressures above 1 MPa to assess for possible particle breakage occurred during the shearing phase. An isotropic compression test at the maximum confining pressure (120 MPa) was also carried out, and a sample was retrieved to evaluate the particle breakage occurrence only due to iron ore tailings isotropic compression. The PSD curves are summarised in Fig. 1 and can be directly compared to the results of the untested tailings.

The PSD curves for specimens sheared at 1.20 MPa and 2 MPa confining pressure tests are similar to the untested material, indicating a low particle breakage for this stress level. Although the PSD curves for these tests are visually similar, they differ slightly, and the semi-logarithmic scale minimizes the differences between them. Besides, by increasing the confining pressures (from 6 MPa up to 120 MPa), the grading curves offset upwards from the untested material curve. As a result, the finer content increases for specimens from tests performed at higher pressures. The particle breakage in the isotropic compression test at 120 MPa was minor compared to the breakage in the test sheared with confining pressure of 6 MPa. Thus, the shearing induced remarkable particle breakage to tailings materials when compared to isotropic compression.

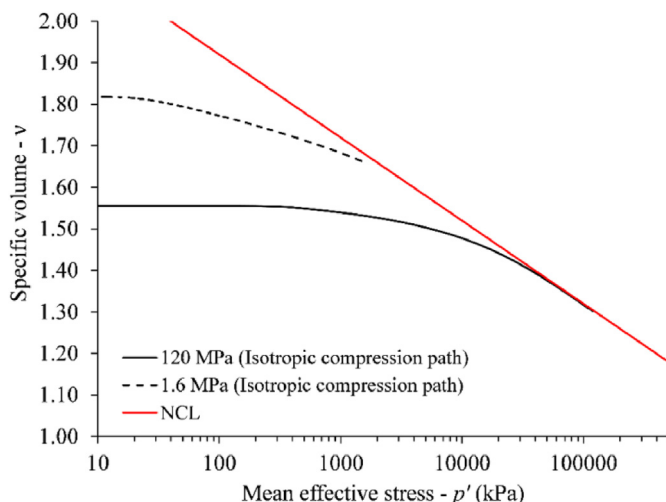


Fig. 4. Isotropic compression behaviour of the iron ore tailings.

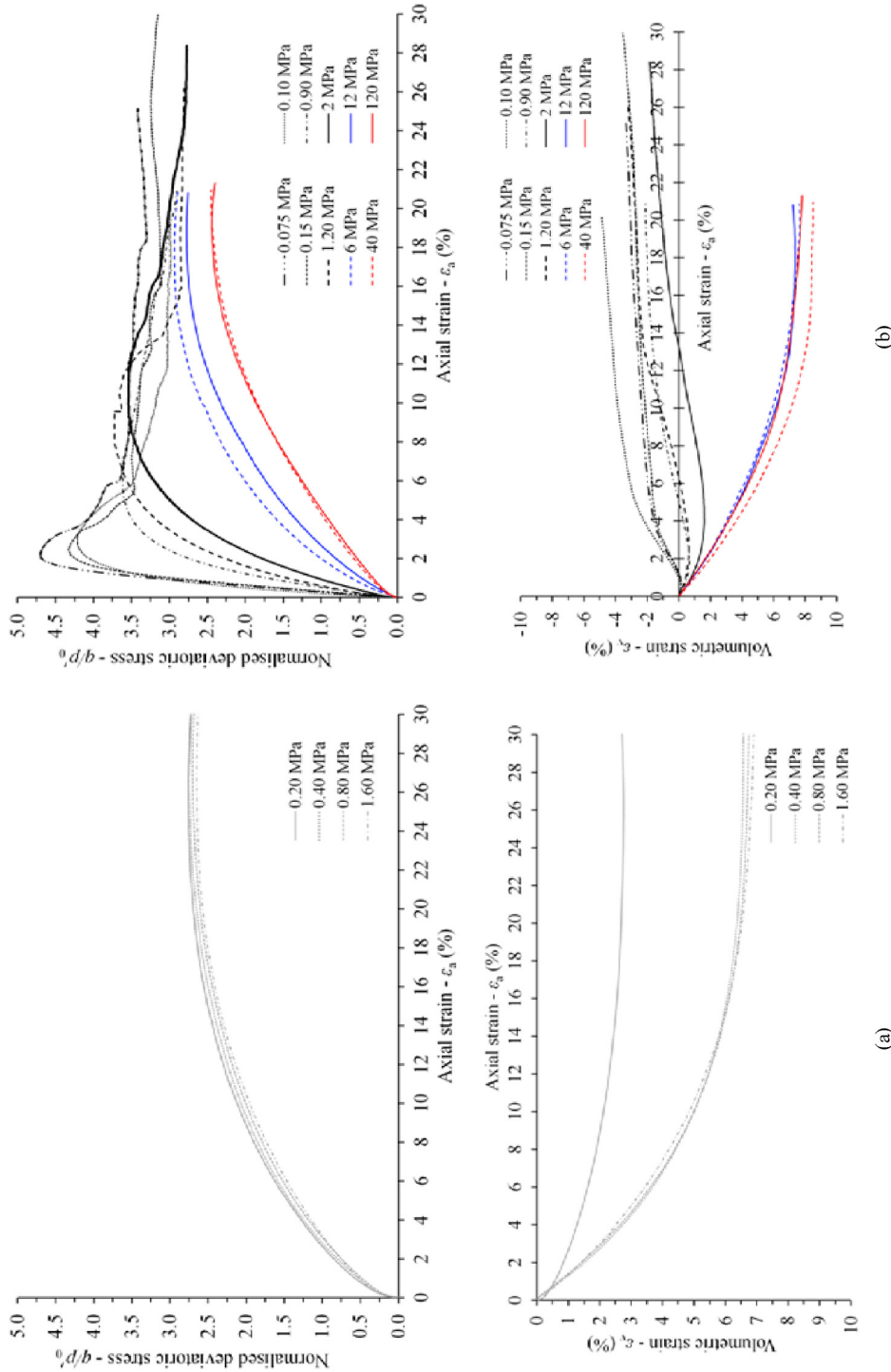
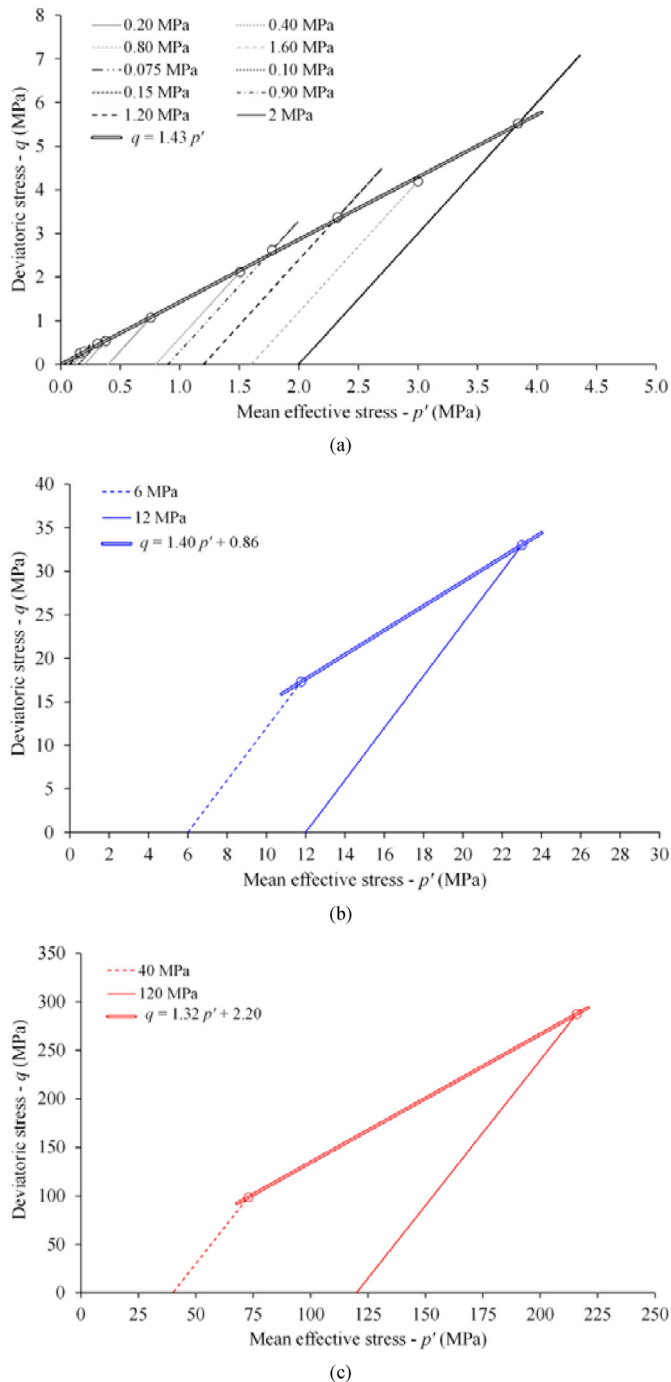


Fig. 5. Stress-strain and volumetric change behaviour for (a) loose tests and (b) dense tests.



**Fig. 6.** Stress paths from (a) low pressures, (b) high pressures, and (c) extremely high pressures.

An adaptation of the relative breakage parameter  $B_r$  (Hardin 1985) was employed to quantitatively assess the amount of breakage. Hardin (1985) limited the lower limit for grain size to 0.074 mm for the index calculation, and herein particles smaller than 0.074 mm appeared to have been broken. Thus, all the grain sizes of the distribution curves were used in the calculation. Fig. 8 compares the areas considered by Hardin with those considered in this work for the  $B_r$  calculation. It is necessary to notice that this method implies some issues. For example, slight differences in the curves for the coarser particles imply more changes in the index (i.e. the area difference is much greater between 1 mm and 10 mm

than that between 0.1 mm and 1 mm, although at a logarithmic scale the distance is the same).

Fig. 9 depicts the relative breakage as a function of the maximum mean effective stress measured during each test. The  $B_r$  value increased with the confining pressures in the sheared samples and was low for the sample submitted only to isotropic compression. The increasing trend in the relative breakage measured is nonlinear with increasing maximum mean effective stresses experienced by the samples during shear. The nonlinearity becomes more evident for the 120 MPa test than for tests up to 12 MPa effective confining stress. After the 12 MPa test, there is a gradual reduction in the breakage increment rate, indicating a possible steadiness of breakage for pressures up to 120 MPa effective confining stress. Other studies have shown similar responses (e.g. Huang et al., 2014; Zhong et al., 2018; Xiao et al., 2019; Zhang et al., 2020). The increase in the mean effective stresses induces more breakage, which results in a higher particle number. Then, this new arrangement provides more contact points between particles. Thus, although the total stress in the particle increases with increasing pressures, the average stress of the contact points declines, and the consequent particle breakage is reduced.

The changes in tailings' particle morphology (seen through SEM micrographs) can be noticed comparing untested specimen in Fig. 2a, and specimen subjected to a confining pressure of 120 MPa in Fig. 2b, followed by shearing. Compared to the untested material (see Fig. 2a), the tailings tested at 120 MPa confining pressures and sheared present a higher fines content (which can be most clearly identified in the PSD curves shown in Fig. 1). No plate-shaped particles were identified after the sample was sheared at 120 MPa, indicating that these particles are more susceptible to breakage and are firstly crushed. However, there still can be identified some bulky particles, although less angular in comparison to the untested sample. The persistence of bulky particles occurs probably due to cushioning, where the smaller particles with higher coordination numbers involve the greater ones, increasing the number of contacts and, thus reducing breakage (Altuhaifi and Coop, 2011).

### 3.4. Data fit in the $v$ - $\ln p'$ plane

The deviatoric stress–axial strain–volumetric strain results obtained are analysed at the compression plane, as shown in Fig. 10. Despite the moulding variability, the specimens start from the two previously defined isotropic compression paths for loose and dense initial conditions. At lower stresses, the loose specimens contract and the dense ones dilate during shear. At higher stresses, the dense specimens contract during shear, indicating a change in the behaviour trend. Initially, it was attempted to fit the data points with a straight line in semi-log space (Schofield and Wroth, 1968):

$$e_c = \Gamma - \lambda \ln p' \quad (1)$$

where  $e_c$  is critical state void ratio,  $\Gamma$  is critical state line intercept, and  $\lambda$  is the slope of critical state line.

This form has not captured the shift in behaviour that occurs under higher pressures and even a noticed nonlinearity at lower stresses. From Fig. 11, a linear trend does not satisfactorily fit the data for iron ore tailings over the entire pressure range. The nonlinear behaviour is expected in some particulate materials at high pressures and is generally associated with the onset of particle breakage (Been et al., 1991; Verdugo, 1992; Coop and Lee, 1993; Yamamuro and Lade, 1996; Luzzani and Coop, 2002; Muir Wood, 2007). However, Bedin et al. (2012), while studying the liquefaction behaviour of gold mine tailings, noticed that the response of particulate materials might be highly nonlinear already at low



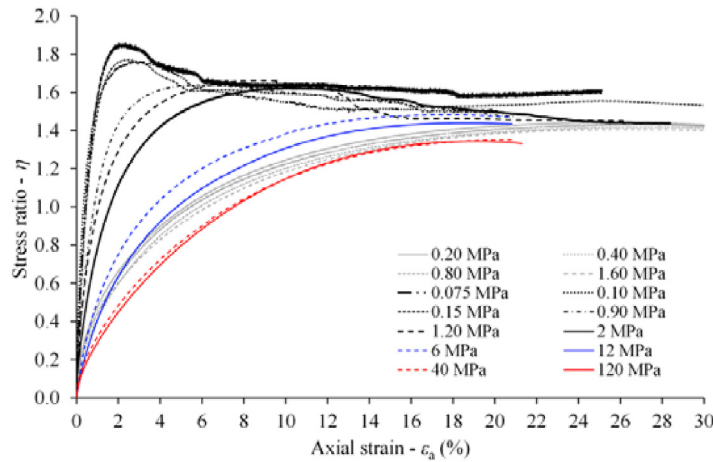


Fig. 7. Stress ratio ( $q/p'$ )–axial strain response.

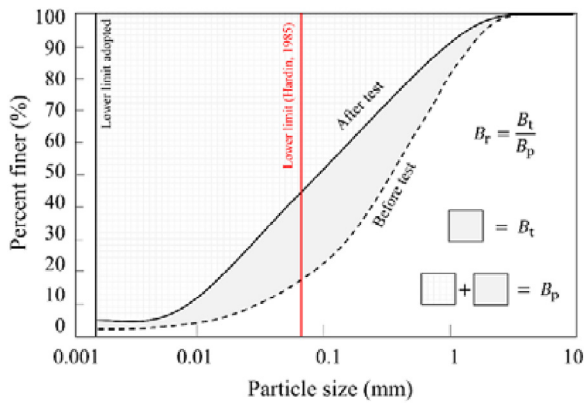


Fig. 8. Procedure used to calculate the relative particle breakage ( $B_r$ ) by total breakage ( $B_t$ ) and breakage potential ( $B_p$ ) values.

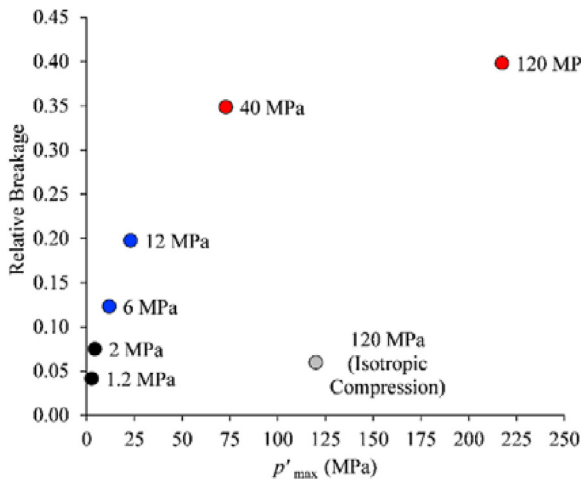


Fig. 9. Relative breakage to different mean effective stresses.  $p'_{max}$  is the maximum mean effective stress the samples experienced.

confining pressures. Hence, it is proposed that the CSL may be nonlinear from low pressures associated with the existence of metastable states that the materials can be in this region of behaviour (Wagner et al., 2023). Although particle breakage may

already initiate at intermediate pressures (as 1.2 MPa observed here), the marked change in slope of the CSL in  $v-\ln p'$  plane is associated with the point in which particle breakage becomes the primary deformation mechanism.

Hence, a curved CSL is required to fit the observed response. This approach presents a better abstraction of behaviour of iron ore tailings because it provides a unique equation defining continuous behaviour along different stress ranges. Gudehus (1996) and Jefferies and Been (2016) proposed closed forms which fit these requirements, respectively, as

$$v = 1 + e_{i0} \exp \left[ - \left( \frac{3p'}{h_s} \right)^n \right] \quad (2)$$

where  $e_{i0}$  is the critical state line intercept,  $h_s$  is the grain hardness, and  $n$  is a material constant, and

$$v = a - b \ln \left( \frac{p'}{p'_{ref}} \right)^c \quad (3)$$

where  $a$  is the critical state line intercept,  $b$  and  $c$  are the fitting parameters, and  $p'_{ref}$  is an arbitrary reference pressure.

Fig. 11 also presents the attempt to fit the experimental data for Eqs. (2) and (3) which fit well with experimental data that reach

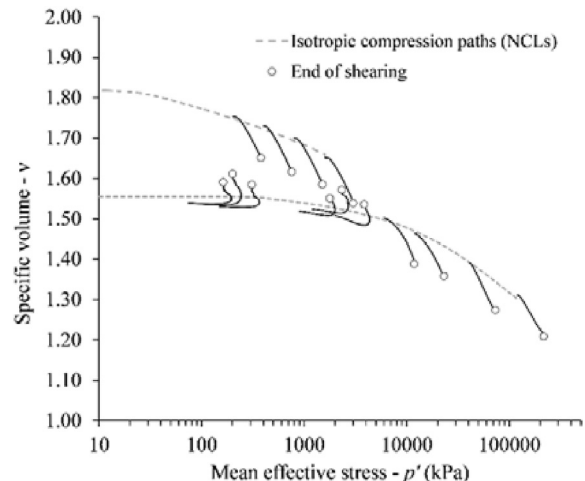
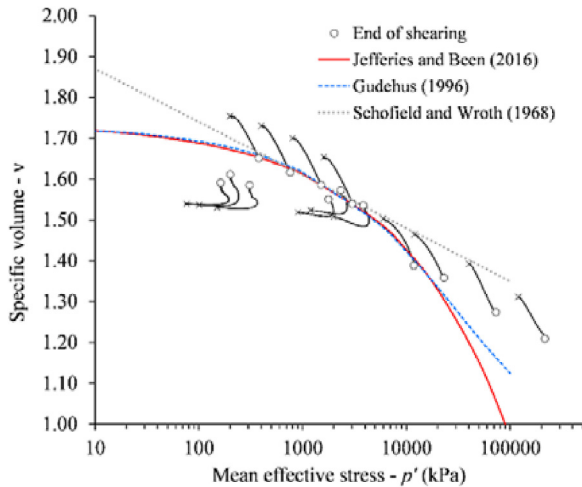


Fig. 10. Triaxial test results at compression plane.



**Fig. 11.** Fitting experimental data for CSL by the equations proposed by Schofield and Wroth (1968), Gudehus (1996), and Jefferies and Been (2016).

mean effective stress close to 12 MPa at the end of shearing. However, the tests that achieved higher mean effective stresses (upper to 12 MPa till 216 MPa at the end of the test) did not show a good fit, and the endpoints were far from the curves proposed by conventional equations. Despite being nonlinear and continuous, the equations do not provide a reduction in slope with increasing pressure, as experimentally observed. A CSL idealisation should account for this reduction in the slope of the volumetric strain curve, as reported in Fig. 5b, that induces a new segment of behaviour. The specimens at such high pressures achieve states of maximum compression owing to elevated amounts of breakage and particle rearrangements. Thus, they cannot further contract or at least show the tendency to stabilise contractive behaviour, producing a flatter portion of CSL.

An idealisation of CSL for the studied silty-sandy materials in the compression plane is proposed in the next section accounting for at least three regions of behaviour:

- (1) A nonlinear, with a gentle slope, portion up to the point in which particle breakage becomes the primary deformation mechanism;
- (2) A steep segment associated with virgin compression and nearly parallel to the NCL (or the limiting normal compression line, LNCL); and
- (3) A flatter portion with asymptotic trend behaviour.

### 3.5. Proposed inverse S-shaped CSL from low to high pressures

An inverse S-shaped CSL equation has its foundations in experimental evidence obtained from laboratory tests on silty-sandy materials' behaviour at high confining pressures. For this, a suitable idealisation should be a continuous function presenting: (i) asymptotic responses near the initial specific volume and at a low specific volume under high pressures, (ii) an intermediate nonlinear behaviour able to represent the onset of crushing, and (iii) a segment where crushing is the primary deformation mechanism.

Mathematically, this shape could be achieved through many forms. This work chose a generalised logistic function that allows a greater parameterisation for a sigmoid function. In this form, it is possible to control the initial portion's inclination, the curve's scale,

and the asymptotic behaviours needed. The usual form of definition of this function is given by

$$f(x) = A + \frac{K - A}{[C + Q \exp(-Bx)]^{1/D}} \quad (4)$$

where  $A$  and  $K$  are the limiting asymptotes; and  $C$ ,  $Q$ ,  $B$ , and  $D$  are the fitting parameters.

Adjustments were made to Eq. (4) to provide a more direct form. Thus, the proposed CSL can be defined by

$$v = v_{\min} + \left[ \frac{C_1 + 1}{C_1 + \exp(-C_2 p' / p'_{\text{ref}})} \right]^{1/C_3} (v_0 - v_{\min}) \quad (5)$$

where  $v_0$  is the limiting (maximum specific volume at critical state that the material could achieve) specific volume;  $v_{\min}$  is the inferior asymptote, related to the minimum specific volume that the material could achieve; and  $C_1$ ,  $C_2$ , and  $C_3$  are the fitting parameters related to the material response. The parameter  $p'_{\text{ref}}$  is herein assumed as 10 MPa.

Although the notation used for  $v_{\min}$  is similar to usual  $e_{\min}$ , it is crucial to separate these two measures clearly. While  $e_{\min}$  is a notation for the minimum void ratio achieved in tests involving vibration and is related to an achievable state of the specimen prior to shearing,  $v_{\min}$  is a parameter proposed in this work to represent a physical limit. The parameter  $v_{\min}$  in Eq. (5), thus, defines the limit in which particle breakage would cease.

Fig. 12 presents the fitting of experimental data to the proposed equation. The coefficient of determination,  $R^2$ , obtained by the fitting parameters was 0.98. The performed tests delimited the CSL over a broad range of confining pressures by the dry and wet sides (lower stresses) and the wet side (higher stresses). The CSL delimitation by the dry side for the higher stresses is challenging due to the constraint of dilation and the high degree of particle breakage for this stress level.

Considering the particle breakage as the only grading changing mechanism, the existence of a limiting NCL delimits the states achievable for a certain material (see Fig. 13). As breakage also occurs during isotropic compression, this NCL evolves along with the CSL. Thus, some degree of grading evolution would be necessary to achieve a given state in terms of stress. This feature gives rise to the importance of defining the CSL in the  $v-\ln p'$  plane in

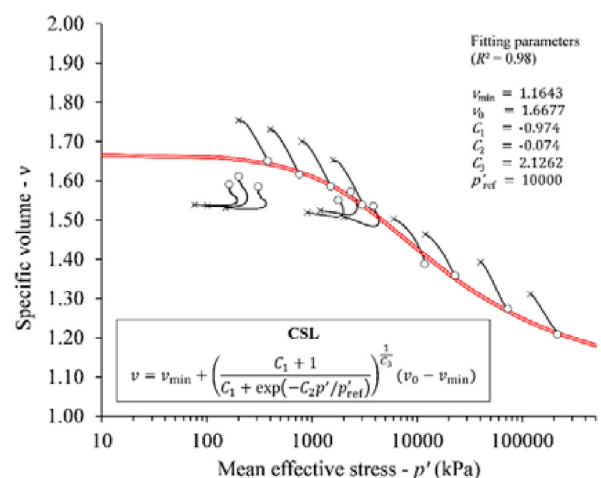


**Fig. 12.** Fitting of the proposed equation for CSL in  $v-\ln p'$  plane for experimental data.

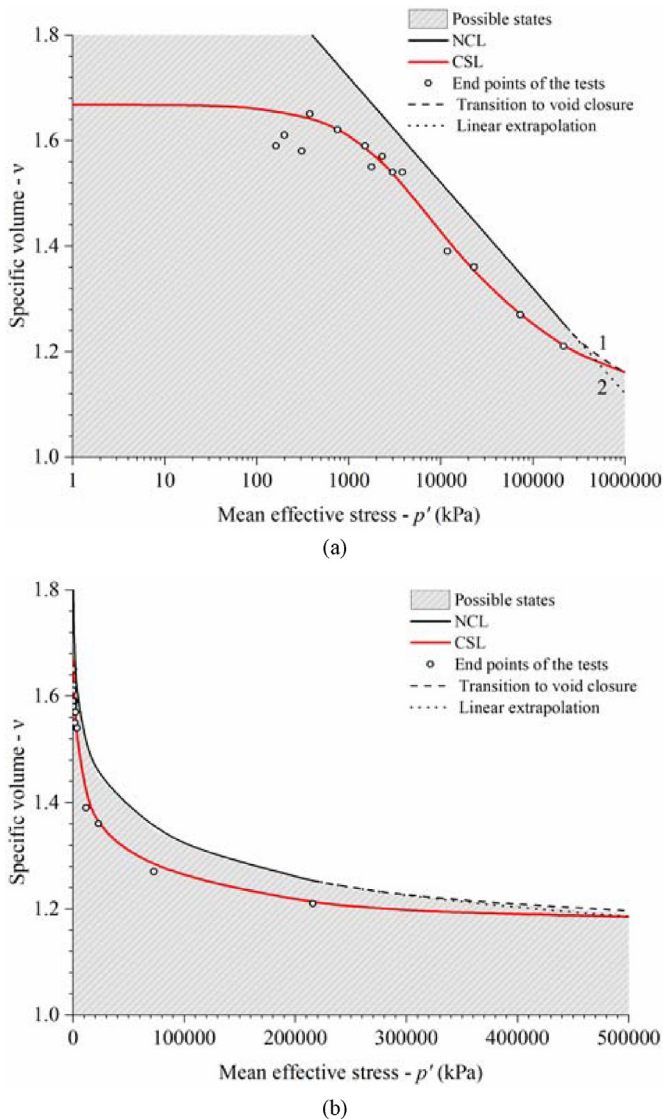


Fig. 13. Relation between the NCL the CSL considering (a) semi-log scale and (b) natural scale.

which it represents the projection (with an inversed S-shaped) of the achievable surface existent for this evolving granular medium.

Fig. 13 also presents the previously defined NCL with the CSL obtained. This NCL was experimentally obtained for confining stresses up to 120 MPa. After this pressure, two proposed behaviours are indicated for the NCL in Fig. 13: (1) A simple linear extrapolation, and (2) a hardening behaviour that tends towards a state of void closure, with asymptotic behaviour (Mun and McCartney 2017). These two possibilities are plotted because further pressures could not be achieved with the apparatus used in this study. Regardless of the considered behaviour for NCL trend (option 1 or 2), a similar conclusion can be drawn for the relationship between the NCL and CSL. When the NCL is assumed to continue linearly, the CSL becomes the limiting surface of achievable states. Otherwise, when the asymptotic behaviour is assumed, the NCL tends towards the defined CSL and, thus the latter also becomes the limiting surface of achievable states. This trend can also be visualised without the semi-log axis usually considered for the compression plane (see Fig. 13b). This form of plotting the CSL and NCL clearly marks the asymptotic trend in both conditions which can be expected to converge or not.

Fig. 14 shows each of the three proposed segments in  $\nu$ - $\ln p'$  plane and their relation to the observed behaviour in particle breakage and  $q$ - $p'$  plane. Each of the segments of the CSL in the compression plane can be associated with a different deformation mechanism and a respective behaviour in other planes. The amount of breakage plays an essential role in the shift of the material response, reflected by the existence of curved CSL in both  $\nu$ - $\ln p'$  and  $q$ - $p'$  planes:

- (1) Section (I): This section includes the samples sheared with confining pressures up to 2 MPa. The grading curves of the tested samples were similar to that of untested material, indicating low particle breakage (relative breakage values of 0.04 to 0.07 for 1.2 MPa and 2 MPa tests). The amount of breakage did not influence the behaviour in other planes. As expected for frictional material, the CSL in the  $q$ - $p'$  plane was linear ( $q/p' = 1.43$ ) with no cohesive intercept till this stress level. At the  $\nu$ - $\ln p'$  plane, a nonlinear trend with a gentle slope was observed since the lower stresses to 2 MPa confining pressure.
- (2) Section (II): This section refers to the samples being sheared with confining pressures of 6 MPa and 12 MPa. The amount of breakage increases and becomes the primary deformation mechanism. The grading curves of the tested samples are away from the untested material (the correspondent relative breakage values are 0.12 and 0.20). The  $q/p'$  ratio reduces to 1.40 and a cohesive intercept of 0.86 MPa arises in the  $q$ - $p'$  plane for this condition, indicating a curvature of the CSL. In addition, a steep section was observed at the  $\nu$ - $\ln p'$  plane for this mean effective stress level.
- (3) Section (III): The last section represents the samples sheared with higher confining pressures (40 MPa and 120 MPa). As a result, the crushing increases significantly and occurs for particles of all sizes, resulting in a higher finer content for sheared samples than that of untested material (the correspondent relative breakage values are 0.35 and 0.40). The cohesive intercept increases to 2.20 MPa, and the  $q/p'$  ratio reduces to 1.32 in the  $q$ - $p'$  plane, demonstrating that the curvature of the CSL in this plane is directly related to the amount of breakage that occurs. At the compression plane ( $\nu$ - $\ln p'$ ), a flatter portion with asymptotic trend behaviour is observed, which corresponds to states of maximum compression due to elevated amounts of breakage and particle rearrangements.

However, it is important to reaffirm that the cohesive intercept arising in sections II and III proposed does not represent a cohesive trend for the iron ore tailings. These values of cohesive intercept are just a consequence of the observed curvature in the CSL at the  $q$ - $p'$  plane, as they arise from the adoption of a linear fitting for a truly nonlinear envelope caused by the occurrence of particle breakage.

#### 4. Conclusions

An experimental study of behaviour of iron ore tailings up to high confining pressures in drained triaxial compression tests was presented. The NCL and CSL of silty-sandy tailings were determined in the entire range of stresses, from small to high confining pressures. The results show that the amount of breakage plays an essential role in the shift of the geomaterial response as the pressures increase and mark the existence of curved CSL in both  $\nu$ - $\ln p'$  and  $q$ - $p'$  planes. The main conclusions of the study are presented below:

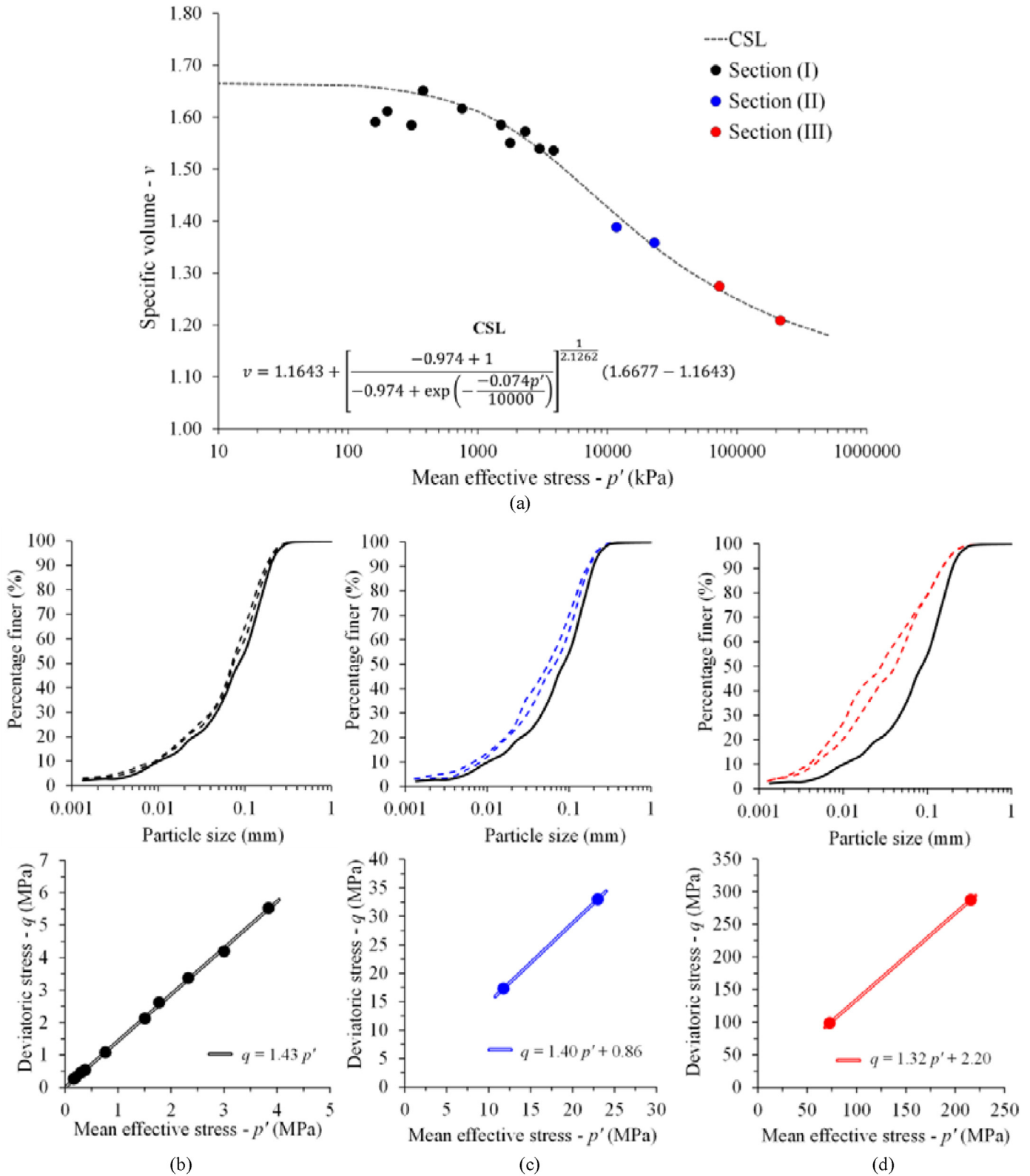


**Fig. 14.** Physical interpretation of the proposed idealised equation for CSL: (a) CSL on  $v-\ln p'$  plane and sections defined; (b) PSD and CSL on  $q-p'$  plane for section (I); (c) PSD and CSL on  $q-p'$  plane for section (II); and (d) PSD and CSL on  $q-p'$  plane for section (III).

- (1) The increase in confining pressure decreases the steepness of the normalised deviatoric stress–axial strain curves, decreases the maximum normalised deviatoric stress reached, and increases the volumetric contraction (there is no dilatancy tendency to higher stresses) up to the point of maximum compression.
- (2) The maximum deviatoric stress increases as the mean effective stress increases. Nevertheless, the material shows a

nonlinear behaviour for the full range of stresses in the  $q-p'$  plane. The nonlinearity of the CSL in this plane arises for confining pressures upper to 2 MPa due to the amount of particle breakage occurring.

- (3) The increase of  $B_r$  is nonlinear with increase of the maximum mean effective stresses. After 12 MPa of confining pressure, the nonlinearity becomes more evident and there is a reduction in the breakage rate, indicating a possible stabilisation for stresses higher than 120 MPa.
- (4) An inverse S-shaped curve was adjusted to experimental results on the  $\nu-\ln p'$  plane. A new equation with five parameters was proposed to represent the behaviour of silty-sandy iron ore tailings in the full range of states it can achieve. This continuous function considers three regions of behaviour. The determination of each segment at the  $\nu-\ln p'$  plane is appropriately related to the observed behaviour in particle breakage and in  $q-p'$  plane. There was a gap concerning propositions that defined the CSL in its full range of states.
- (5) The pressures studied here were much higher than those previewed to occur in the field dry stack problems and aimed to understand the full influence of particle breakage in intermediate soil behaviour. The definition of the full range of behaviour for iron ore tailings helps engineers in key decision issues once they know in which segment of behaviour they are working.

#### Data availability

The data that support the findings of this study are available from the corresponding author upon reasonable request.

#### Declaration of competing interest

The authors declare that they have no known competing financial interests or personal relationships that could have appeared to influence the work reported in this paper.

#### Acknowledgements

The Universidade Federal do Rio Grande do Sul supported the experimental work performed at Vale's Geotechnical Laboratory (LGV). The authors wish to express their appreciation to VALE S.A., MEC-CAPES (PROEX), and the Brazilian Research Council (CNPq) for the support of the research group.

#### List of symbols

$B_r$	Relative breakage parameter
$C_u$	Coefficient of uniformity
$C_{cu}$	Coefficient of curvature
$e$	Void ratio
$e_{\min}$	Minimum void ratio
$e_{\max}$	Maximum void ratio
$h_s$	Grain hardness parameter
$G_s$	Specific gravity
$\phi'$	Friction angle
$\gamma$	Specific weight
$\Gamma$	Intercept of CSL at compression plane
$\nu$	Specific volume ( $= 1 + e$ )
$\nu_{\min}$	Lower horizontal asymptote for CSL at compression plane
$\nu_0$	Upper horizontal asymptote for CSL at compression plane
$\nu_i$	Specific volume prior to shearing
$\eta$	Stress ratio $= q/p'$

$\lambda$  Slope of CSL at compression plane  $p'$  Slope of CSL at compression plane/ $\nu$  Mean effective stress

$p'_0$  Mean effective stress at the beginning of the shearing phase

$q$  Deviatoric stress ( $= \sigma_1 - \sigma_3$ )

$\sigma'_1, \sigma'_3$  Principal effective stresses

$\epsilon_a$  Axial strain

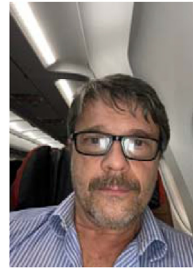
$\epsilon_v$  Volumetric strain

$w$  Water content

#### References

- Ahmadi-Naghadeh, R., Toker, N.K., 2017. Volume change measurement in triaxial tests by monitoring cell fluid volume based on viscoelastic behavior of the test setup. *Geotech. Test J.* 40, 20160093.
- ASTM D854-14, 2014. Standard Test Methods for Specific Gravity of Soil Solids by Water Pycnometer. ASTM International, West Conshohocken, PA, USA.
- ASTM D4253-16, 2016. Standard Test Methods for Maximum Index Density and Unit Weight of Soils Using a Vibratory Table. ASTM International, West Conshohocken, PA, USA.
- ASTM D4254-16, 2016. Standard Test Methods for Minimum Index Density and Unit Weight of Soils and Calculation of Relative Density. ASTM International, West Conshohocken, PA, USA.
- ASTM D2487-17, 2017. Standard Practice for Classification of Soils for Engineering Purposes (Unified Soil Classification System). ASTM International, West Conshohocken, PA, USA.
- ASTM D4318-17, 2017. Standard Test Methods for Liquid Limit, Plastic Limit, and Plasticity Index of Soils. ASTM International, West Conshohocken, PA, USA.
- ASTM D698-21, 2021. Standard Test Methods for Laboratory Compaction Characteristics of Soil Using Standard Effort (12,400 Ft-Lbf/ft<sup>3</sup> (600 kN-M/m<sup>3</sup>)). ASTM International, West Conshohocken, PA, USA.
- ASTM D1557-21, 2021. Standard Test Methods for Laboratory Compaction Characteristics of Soil Using Modified Effort (56,000 Ft-Lbf/ft<sup>3</sup> (2,700 kN-M/m<sup>3</sup>)). ASTM International, West Conshohocken, PA, USA.
- ASTM D7928-21, 2021. Standard Test Method for Particle-Size Distribution (Gradation) of Fine-Grained Soils Using the Sedimentation (Hydrometer) Analysis. ASTM International, West Conshohocken, PA, USA.
- Been, K., Jefferies, M., 1985. A state parameter for sands. *Geotechnique* 35, 99–112.
- Been, K., Jefferies, M., Hachey, J., 1991. The critical state of sands. *Geotechnique* 41, 365–381.
- Consoli, N.C., 1991. Numerical Modelling of the Sedimentation and Consolidation of Tailings. PhD Thesis. Concordia University, Canada.
- Consoli, N.C., Heineck, K.S., Coop, M.R., da Fonseca, A.V., Ferreira, C., 2007. Coal bottom ash as a geomaterial: influence of particle morphology on the behavior of granular materials. *Soils Found.* 47, 361–373.
- Consoli, N.C., Vogt, J.C., Silva, J.P.S., et al., 2022. Behaviour of compacted filtered iron ore tailings—Portland cement blends: new Brazilian trend for tailings disposal by stacking. *Appl. Sci.* 12, 836.
- Coop, M.R., 1990. The mechanics of uncemented carbonate sands. *Geotechnique* 40, 607–626.
- Coop, M.R., Lee, I.K., 1993. The behaviour of granular soils at elevated stresses. In: *Predictive Soil Mechanics. Proceedings of the Wroth Memorial Symposium.* Thomas Telford Ltd, Oxford, pp. 186–198.
- Corrêa, M.M., Oliveira Filho, W.L., 2019. Impact of methods used to reconstitute tailings specimens on the liquefaction potential assessment of tailings dams. *REM, Int. Eng. J.* 72, 507–513.
- Dafalias, Y.F., Manzari, M.T., 2004. Simple plasticity sand model accounting for fabric change effects. *J. Eng. Mech.* 130, 622–634.
- Davies, M., 2011. Filtered dry stacked tailings: the fundamentals. In: *Proceedings of the Tailings and Mine Waste Conference.* The University of British Columbia, Vancouver, Canada.
- Gajo, A., Muir Wood, D., 1999a. A kinematic hardening constitutive model for sands: the multi-axial formulation. *Int. J. Numer. Anal. Methods GeoMech.* 23, 925–965.
- Gajo, A., Muir Wood, D., 1999b. Severn-Trent sand: a kinematic-hardening constitutive model: the  $q-p$  formulation. *Geotechnique* 49, 595–614.
- Gudehus, G., 1996. A comprehensive constitutive equation for granular materials. *Soils Found.* 36, 1–12.
- Hardin, B.O., 1985. Crushing of soil particles. *J. Geotech. Engrg.* 111, 1177–1192.
- Huang, J., Xu, S., Hu, S., 2014. Influence of particle breakage on the dynamic compression responses of brittle granular materials. *Mech. Mater.* 68, 15–28.
- Jefferies, M., Been, K., 2016. In: *Soil Liquefaction: A Critical State Approach*, second ed. CRC Press, London, UK.
- Leung, C.F., Lee, F.H., Yet, N.S., 1996. The role of particle breakage in pile creep in sand. *Can. Geotech. J.* 33, 888–898.
- Lupo, J., Hall, J., 2011. Dry Stack tailings—design considerations. In: *Tailings and Mine Waste '10: Proceedings of the 14th International Conference on Tailings and Mine Waste*, Vail, Colorado, USA, 17–20 October 2010. Presented at the Tailings and Mine Waste Conference. CRC Press, Boca Raton, USA.
- Luzzani, L., Coop, M.R., 2002. On the relationship between particle breakage and the critical state of sands. *Soils Found.* 42, 71–82.

- Muir Wood, D., 2007. The magic of sands—The 20th Bjerrum Lecture. *Can. Geotech. J.* 44, 1329–1350.
- Muir Wood, D., Maeda, K., 2008. Changing grading of soil: effect on critical states. *Acta Geotech* 3, 3–14.
- Muir Wood, D., 2017. Geomaterials with changing grading: a route towards modelling. In: Hyodo, M., Murata, H., Nakata, Y. (Eds.), *Geomechanics and Geotechnics of Particulate Media*. CRC Press, Boca Raton, USA, pp. 313–318.
- Mun, W., McCartney, J.S., 2015. Compression mechanisms of unsaturated clay under high stresses. *Can. Geotech. J.* 52. <https://doi.org/10.1139/cgj-2014-043>.
- Mun, W., McCartney, J.S., 2017. Roles of particle breakage and drainage in the isotropic compression of sand to high pressures. *J. Geotech. Geoenviron. Eng.* 143, 04017071.
- Poorooshasb, H.B., 1989. Description of flow of sand using state parameters. *Comput. Geotech.* 8, 195–218.
- Roscoe, K.H., Schofield, A.N., Wroth, C.P., 1958. On the yielding of soils. *Geotechnique* 8, 22–53.
- Russell, A.R., Khalili, N., 2004. A bounding surface plasticity model for sands exhibiting particle crushing. *Can. Geotech. J.* 41. <https://doi.org/10.1139/t04-065>.
- Schofield, A., Wroth, C.P., 1968. *Critical State Soil Mechanics*. McGraw-Hill, New York, USA.
- Suits, L.D., Sheahan, T., Frost, J., Park, J.-Y., 2003. A critical assessment of the moist tamping technique. *Geotech. Test J.* 26, 9850.
- Verdugo, R., 1992. Discussion: the critical state of sands. *Geotechnique* 42, 655–663.
- Wagner, A.C., Silva, J.P. de S., Carvalho, J.V. de A., et al., 2023. Mechanical behavior of iron ore tailings under standard compression and extension triaxial stress paths. *J. Rock Mech. Geotech. Eng.* 15, 1883–1894.
- Wroth, C.P., Bassett, R.H., 1965. A stress–strain relationship for the shearing behaviour of a sand. *Geotechnique* 15, 32–56.
- Wu, D., 2020. Solutions for surface disposal of mine tailings. In: *Mine Waste Management in China: Recent Development*. Springer Singapore, Singapore, pp. 11–19.
- Xiao, Y., Liu, H., Ding, X., et al., 2016. Influence of particle breakage on critical state line of rockfill material. *Int. J. GeoMech.* 16, 04015031.
- Xiao, Y., Long, L., Matthew Evans, T., et al., 2019. Effect of particle shape on stress-dilatancy responses of medium-dense sands. *J. Geotech. Geoenviron. Eng.* 145, 04018105.
- Yamamoto, J.A., Lade, P.V., 1996. Drained sand behavior in axisymmetric tests at high pressures. *J. Geotech. Eng.* 122, 109–119.
- Yu, H.-S., 1998. CASM: a unified state parameter model for clay and sand. *Int. J. Numer. Anal. Methods GeoMech.* 22, 621–653.
- Yu, F., 2021. Particle breakage in granular soils: a review. *Part. Sci. Technol.* 39, 91–100.
- Zhang, C., Chen, Q., Pan, Z., Ma, C., 2020. Mechanical behavior and particle breakage of tailings under high confining pressure. *Eng. Geol.* 265, 105419.
- Zhong, W., Yue, F., Ciancio, A., 2018. Fractal behavior of particle size distribution in the rare earth tailings crushing process under high stress condition. *Appl. Sci.* 8, 1058.



**Professor Nilo Cesar Consoli** is presently working as a Scientist/Professor at Graduate Program in Civil Engineering at Universidade Federal University do Rio Grande do Sul (UFRGS), Brazil. He is a Scientist listed among the 1% most influential in the world according to studies developed in September 2022 by Stanford University, USA. He is innovation consultant for VALE (Brazilian Mining Company) and PETROBRAS (Brazilian Oil Company). He obtained his PhD in Civil Engineering at Concordia University, Canada in 1991, carried out postdoctoral research at University of Oxford (1996) and The University of Western Australia (2006). He is Associate Editor of *ASCE Journal of Geotechnical and Geoenvironmental Engineering* and *ASCE Journal of Materials in Civil Engineering*. He also is Editorial Board Member of *Canadian Geotechnical Journal*, and *Transportation Geotechnics*. He was awarded with Telford Prize (2001) and Telford Premium (2009) by The Institution of Civil Engineers, UK. Professor Consoli has published 260 peer-reviewed papers indexed in Scopus (8204 citations and h-index 50). Professor Consoli has experience in Geotechnical and Geoenvironmental Engineering and Sustainability, acting on the following subjects: Mine tailings stacking, development of new geomaterials, three pillars of sustainability, nanomaterials, constitutive modelling, artificially cemented geomaterials, and reuse of wastes for soil stabilisation.